

Quench dynamics of Anderson-localized interacting exciton-polaritons

Zhi-Hao Sun(孙志豪), Yong-Jia Chong(冲勇嘉), Yu Guan(管煜), Zheng-Ye Wang(王正叶), Meng Chen(陈猛), Lei Chen(陈雷), and Xingran Xu(许星然)

Citation: Chin. Phys. B, 2026, 35 (**5**): 057106. DOI: 10.1088/1674-1056/ae4e87
http://cpb.iphy.ac.cn; http://iopscience.iop.org/cpb

What follows is a list of articles you may be interested in

A two-stage injection locking amplifier based on a cavity magnonic oscillator

Mun Kim, Chunlei Zhang, Chenyang Lu, Jacob Burgess, and Can-Ming Hu

Chin. Phys. B, 2025, 34 (**6**): 067104. DOI: 10.1088/1674-1056/add1bf

Actively tuning anisotropic light—matter interaction in biaxial hyperbolic material α-MoO_3 using phase change material VO_2 and graphene

Kun Zhou(周昆), Yang Hu(胡杨), Biyuan Wu(吴必园), Xiaoxing Zhong(仲晓星), and Xiaohu Wu(吴小虎)

Chin. Phys. B, 2024, 33 (**4**): 047103. DOI: 10.1088/1674-1056/ad23d2

Exciton-polaritons in a 2D hybrid organic-inorganic perovskite microcavity with the presence of optical Stark effect

Kenneth Coker, Chuyuan Zheng(郑楚媛), Joseph Roger Arhin, Kwame Opuni-Boachie Obour Agyekum, and Weili Zhang(张伟利)

Chin. Phys. B, 2024, 33 (**3**): 037102. DOI: 10.1088/1674-1056/ad1484

Polarization-dependent ultrafast carrier dynamics in GaAs with anisotropic response

Ya-Chao Li(李亚超), Chao Ge(葛超), Peng Wang(汪鹏), Shuang Liu(刘爽), Xiao-Ran Ma(麻晓冉), Bing Wang(王冰), Hai-Ying Song(宋海英), and Shi-Bing Liu(刘世炳)

Chin. Phys. B, 2022, 31 (**6**): 067102. DOI: 10.1088/1674-1056/ac422b

---

SPECIAL TOPIC — Exciton physics: Fundamentals, materials and devices

Quench dynamics of Anderson-localized interacting exciton-polaritons

Zhi-Hao Sun(孙志豪)[1], Yong-Jia Chong(冲勇嘉)[1], Yu Guan(管煜)[1], Zheng-Ye Wang(王正叶)[1], Meng Chen(陈猛)[1], Lei Chen(陈雷)[2,†], and Xingran Xu(许星然)[1,‡]

[1] *School of Science, Jiangnan University, Wuxi* 214122, *China*

[2] *School of Information, Hunan University of Humanities, Science and Technology, Loudi* 417000, *China*

(Received 4 December 2025; revised manuscript received 1 March 2026; accepted manuscript online 7 March 2026)

Exciton–polaritons, formed through strong coupling between photons and excitons, exhibit unique characteristics such as an extremely small effective mass and a propensity to form Bose–Einstein condensates. The dynamics of these condensates are governed by a coupled system of equations that describe the condensate wavefunction and the excitonic reservoir density. Using imaginary-time evolution, the ground state of the condensate in a quasi-periodic potential is determined, revealing a transition from localized to delocalized states as the nonlinearity increases. After quenching the interaction strength, localized condensates with weak nonlinearity propagate without significant distortion, whereas those with strong nonlinearity exhibit breathing-like oscillations. Higher reservoir decay rates promote localization and suppress chaotic behavior, highlighting the interplay between nonlinearity and dissipation in determining the system's dynamical behavior.

Keywords: exciton-polariton, quench dynamics, chaos

PACS: 71.36.+c, 05.45.–a, 72.15.Rn, 03.65.Yz

DOI: 10.1088/1674-1056/ae4e87 **CSTR:** 32038.14.CPB.ae4e87

1. Introduction

Exciton–polaritons, quasiparticles arising from the strong coupling between photons and excitons in semiconductor microcavities, have established themselves as a prototypical platform for studying non-equilibrium quantum fluids of light.[1–3] Their inherently driven–dissipative nature — requiring continuous optical pumping to compensate for photon loss — places them fundamentally out of thermodynamic equilibrium. This unique setting gives rise to a rich spectrum of phenomena not found in closed conservative systems, including non-Hermitian physics with exceptional points,[4–7] the formation of non-equilibrium Bose–Einstein condensates (BECs) even at elevated temperatures,[8–13] and the emergence of dissipative solitons and nonlinear wave patterns.[14,15] The experimental relevance of this platform is further enhanced by a versatile experimental toolbox, encompassing static potentials, all-optical lattices, strain engineering, and metasurfaces supporting bound states in the continuum,[16–27] which allows for precise sculpting of the polariton landscape, enabling exploration of artificial topological matter[28,29] and novel transport regimes such as the non-Hermitian skin effect.[30–32]

Quench dynamics in exciton–polariton condensates — triggered by abrupt changes in interaction strength, pump power, or cavity detuning — further probe how these open-dissipative quantum fluids evolve far from equilibrium, revealing nonlinear phenomena such as dispersive shock waves, soliton trains, parametric amplification, vortex nucleation, quantum turbulence, and Kibble–Zurek-like defect formation.[33–36] Central to this dynamical richness is the interplay between coherent nonlinear interactions and incoherent dissipative processes. Nonlinearity, stemming from polariton–polariton interactions, is the driving mechanism for a plethora of complex behaviors: it facilitates soliton formation, drives parametric instabilities, and underlies quantum turbulence.[37–40] Conversely, dissipation, primarily through cavity photon leakage and reservoir exciton decay, acts as a source of damping and decoherence. In such a competition between nonlinearity and dissipation, the conventional understanding, supported by previous studies of open quantum systems such as polaritonic or cold-atom systems coupled to external baths, has largely cast dissipation in the role of a stabilizer or a suppressor of chaos.[41,42] The prevailing expectation is that strong dissipation dampens fluctuations, suppresses the phase-space exploration necessary for chaotic motion, and ultimately drives the system towards regular, predictable dynamics or steady states, thereby framing dissipation as a passive, calming influence that counters the destabilizing tendencies of strong nonlinearity.

However, this established paradigm immediately raises a

†Corresponding author. E-mail: chenlei@alum.imr.ac.cn

‡Corresponding author. E-mail: thoexxr@hotmail.com

© 2026 Chinese Physical Society and IOP Publishing Ltd. All rights, including for text and data mining, AI training, and similar technologies, are reserved.

critical question: could dissipation, under specific conditions and in concert with nonlinearity, play a more active, constructive, and even chaos-enhancing role? In other words, is the dynamic interplay between nonlinearity (g) and dissipation ($\bar{\gamma}_{\rm R}$) merely competitive, or can it become cooperative, opening up new pathways to instability and chaos that are inaccessible in either the purely conservative or the strongly overdamped limits? Addressing this question is not only of fundamental importance for advancing our understanding of open quantum system dynamics but also crucial for applications seeking to harness or control chaotic behavior in photonic and polaritonic devices, such as chaotic encryption, ultrafast signal processing, quantum simulation, and information processing.

Signatures of Anderson localization in exciton–polariton systems have been experimentally demonstrated in disordered microcavities, most notably through steady-state localization of two-dimensional polariton condensates under controlled disorder.[43] Theoretical investigations have further examined localization–delocalization transitions in quasi-periodic potentials, primarily focusing on ground-state properties and multistable self-trapping.[44] While previous studies focused on static Anderson-localized states or steady-state localization in polariton condensates, the present work investigates the unexplored territory of real-time quench dynamics after a localization–delocalization transition in a quasi-periodic potential.

In this work, we challenge the conventional view by theoretically demonstrating that moderate dissipation can cooperatively interact with nonlinearity to significantly lower the threshold for chaos and expand its parameter regime in an exciton–polariton condensate. We investigate the quench dynamics of an Anderson-localized exciton–polariton condensate in a one-dimensional quasi-periodic potential — a setting that intrinsically hosts both localized and delocalized quantum states. By abruptly switching off the interparticle interaction strength and numerically solving the coupled, dissipative Gross–Pitaevskii equations for the condensate and its excitonic reservoir, we map the ensuing spatiotemporal evolution.

Our key finding is the existence of a cooperative control mechanism governed by the dimensionless interaction strength g and the reservoir decay rate $\bar{\gamma}_{\rm R}$. Contrary to the simplistic picture of dissipation as a universal stabilizer, we show the following results.

Moderate dissipation (intermediate $\bar{\gamma}_{\rm R}$) can synergize with nonlinearity to promote and sustain chaotic dynamics, making chaos more robust and accessible at lower nonlinearities.

A chaotic phase with a large positive maximal Lyapunov exponent emerges in a broad, well-defined window of the (g, $\bar{\gamma}_{\rm R}$) parameter space.

Only very strong dissipation suppresses chaos, whereas weak dissipation or strong nonlinearity alone may not be sufficient to induce it; the joint action of both parameters is decisive.

This cooperative g–$\bar{\gamma}_{\rm R}$ control represents a significant departure from the expected behavior in closed nonlinear systems or strongly damped open systems. It reveals that dissipation can act as a "chaos generator" within a balanced dynamic regime, reshaping the phase diagram and offering a novel, deterministic knob to switch between regular and chaotic evolution.

Therefore, our study shifts the perspective from viewing dissipation merely as a nuisance or a stabilizing agent to recognizing its potential as an active and tunable ingredient for engineering quantum fluid dynamics. The manuscript is structured as follows: In Section 2, we detail the theoretical model of a reservoir-coupled polariton condensate in a quasi-periodic potential. Section 3 presents our numerical results. We first identify the localization–delocalization transition of the ground state (Subsection 3.1), then analyze the quench-induced spatiotemporal dynamics (Subsection 3.2), temporal correlations and power spectra (Subsection 3.3), and finally quantify the chaos through the maximal Lyapunov exponent to construct a phase diagram (Subsection 3.4). Section 4 discusses the implications of our findings, emphasizing the cooperative mechanism and its significance for controlling chaos in open quantum systems.

2. Theoretical model

We examine a one-dimensional exciton–polariton condensate coupled to an excitonic reservoir. The system is subject to external optical pumping, which injects particles into the condensate through both spontaneous and stimulated electronic scattering processes. The temporal and spatial evolution of the condensate wavefunction $\Psi(x,t)$ and the exciton reservoir density $n_{\rm R}(x,t)$ are governed by the generalized stochastic Gross–Pitaevskii (GP) equation and the rate equation as follows:[45,46]

$$\mathrm{i}\hbar\frac{\partial\Psi}{\partial t}=\left[-\frac{\hbar^2}{2M}\frac{\partial^2}{\partial x^2}+V(x)+U(x,t)+\frac{\mathrm{i}\hbar}{2}\left(Rn_{\rm R}-\gamma_{\rm C}\right)\right]\Psi, \tag{1}$$

$$\frac{\partial n_{\rm R}}{\partial t}=-\left(\gamma_{\rm R}+R|\Psi|^2\right)n_{\rm R}+P(x,t), \tag{2}$$

where M represents the effective polariton mass, $V(x)$ denotes the trapping potential, and $U(x,t)=g_{\rm C}|\Psi|^2+g_{\rm R}n_{\rm R}$ is an effective potential. In this expression, $g_{\rm C}$ quantifies the strength of the nonlinear interaction between polaritons, while $g_{\rm R}$ characterizes the coupling strength of the condensate to the reservoir. $P(x,t)$ corresponds to the pump intensity, R describes the rate of stimulated scattering of excitons from the reservoir

into the condensate, and γ_C and γ_R represent the decay rates of cavity photons and reservoir excitons, respectively. For the one-dimensional polariton system under consideration, the parameters γ_C, γ_R, and R have been rescaled by the thickness of the nanowire d as $g_C \to g_C/\sqrt{2\pi d}$, $g_R \to g_R/\sqrt{2\pi d}$, and $R \to R/\sqrt{2\pi d}$.

In this paper, we consider the trapping potential $V(x)$ as a quasiperiodic potential to analyze the characteristics and dynamics of condensate localization. Experimentally, such a potential can be realized through the superposition of two counterpropagating laser beams with slightly different wavelengths, yielding the following form:[47]

$$V(x) = \frac{4\pi^2 s_1}{\lambda_1^2}\cos^2\left(\frac{2\pi x}{\lambda_1}\right) + \frac{4\pi^2 s_2}{\lambda_2^2}\cos^2\left(\frac{2\pi x}{\lambda_2}\right), \quad (3)$$

where $s_1\,(\lambda_1)$ and $s_2\,(\lambda_2)$ represent the amplitudes (wavelengths) of the primary and secondary optical lattices, respectively. For experimental implementation, we set $\lambda_1 = 1032$ nm and $\lambda_2 = 862$ nm. These values are adopted from experimental and theoretical studies of localization in ultracold BECs,[47] directly matching setups with counterpropagating lasers (e.g., for ^{39}K atoms near a Feshbach resonance). They correspond to typical, accessible conditions in state-of-the-art exciton–polariton platforms, such as all-optical lattices in GaAs microcavities, enabling quasi-periodic disorder tunable via laser detuning for room-temperature operation.

By introducing the natural scaling units of the healing length, $x_h = \hbar/(Mc_s)$, and time $\tau_0 = x_h/c_s$, the governing equations are cast into a dimensionless form. This procedure leads to the dimensionless parameters $\bar{\gamma}_C = \hbar\gamma_C/(g_C n_C^*)$ and $\bar{R} = \hbar R/g_C$, where $c_s = \sqrt{g_C n_C^*/M}$ is the local sound velocity in the condensate. The resulting dimensionless equations are given by[48]

$$\mathrm{i}\frac{\partial\psi}{\partial t} = \left(-\frac{1}{2}\frac{\partial^2}{\partial x_h^2} + V(x_h) + g|\psi|^2 + \bar{g}_R m_R + \frac{\mathrm{i}}{2}\bar{R}m_R\right)\psi, \quad (4)$$

$$\frac{\partial m_R}{\partial t} = \bar{\gamma}_C(1-|\psi|^2) - \bar{\gamma}_R m_R - \bar{R}|\psi|^2 m_R, \quad (5)$$

where we have used the fact that $\bar{\gamma}_R = \bar{R}/(P_0/P_{th} - 1)$, which follows from the definition of the dimensionless parameters and the steady-state condition. Moreover, we take $\bar{g} = g/g_C$ and $\bar{g}_R = 2\bar{g}$, and we drop the overline on $\bar{g}$ for notational simplicity. These equations provide the foundation for analyzing the formation, propagation, and stability of nonlinear excitations in driven-dissipative polariton condensates within a well-defined theoretical framework.

3. Results

In this section, the detailed numerical results of the ground states and their related dynamics are presented. For the present analysis, the quasi-periodic potential is employed to investigate the dynamics of the exciton–polariton condensate after the sudden extinction of the initial ground state, whether localized or delocalized. The structure of theis section is as follows: In Subsection 3.1 (ground states), the ground state of the condensate is determined using imaginary-time evolution, and the effect of nonlinearity on localized states in a quasi-periodic potential is investigated. A transition from localized to delocalized states is quantified by analyzing the density distribution profiles as g is increased. In Subsection 3.2 (quench dynamics), dynamical simulations are conducted to explore the emergence of chaos triggered by quenching the interaction strength. The spatiotemporal evolution of the condensate density is mapped for various g and $\bar{\gamma}_R$. In Subsection 3.3 (correlation and dynamical behaviors), the influence of nonlinear interactions and dissipative effects on the transition to chaotic dynamics is probed using the time-correlator function $c(t)$. The power spectral density (PSD) of $c(t)$ is computed to gain a deeper understanding of the chaotic dynamics. In Subsection 3.4 (Lyapunov exponent), the presence of temporal chaos is quantitatively assessed by calculating the maximal Lyapunov exponent (λ_{max}). A chaos phase diagram is constructed to reveal the profound link between localization and chaotic dynamics, demonstrating the competitive mechanism between interactions and dissipation.

3.1. Ground states

In this subsection, we first utilize imaginary-time evolution to determine the conservative ground state (in the absence of the reservoir, $n_R = 0$), with a Gaussian wave packet centered at $x = 0$ selected as the initial condition.[49–51] At each time step, the wave function is normalized to ensure that $\int |\psi|^2 \mathrm{d}x = 1$, and hard-wall boundary conditions $\psi(0) = \psi(N_x - 1) = 0$ are imposed. This reservoir-free calculation isolates the effect of the nonlinear interaction strength g on localization within the quasiperiodic potential $V(x)$, allowing us to examine the fundamental competition between disorder and interactions.

The ground-state density distributions for varying interaction strengths are shown in Fig. 1. In the non-interacting limit ($g = 0$), the condensate is confined to $-5 \le x \le 5$, peaking near $x \sim \pm 2$. As g increases to 4, the wave function develops strong localization at $x = 0$ with an exponential tail, as confirmed by semilogarithmic analysis. However, beyond a critical threshold ($g \ge 5$), matter-wave localization breaks down. This signifies a transition to a delocalized state, where the wave function extends across the entire computational domain bounded by the hard walls, rather than being confined within the potential minima. This is evident in Fig. 1(a), where profiles for $g = 5$ (brown) and $g = 6$ (pink) extend across the computational domain. Figure 1(b) further highlights the exponential decay in the localized regime.

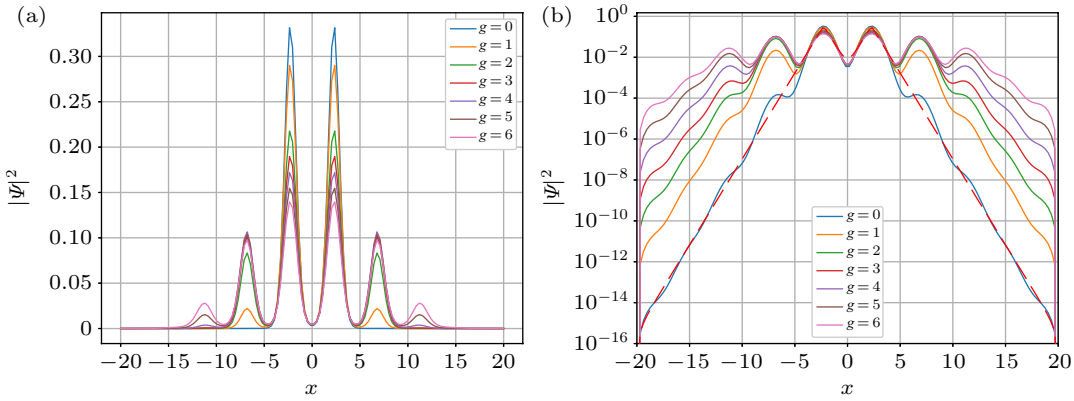


Fig. 1. Variation of the density for different g values in (a) linear and (b) semilogarithmic scales. The wave function is localized near $x = 0$ at $g = 0$. As the nonlinearity increases, the wave function spreads out. In the localized regime ($g = 0, 1, 2, 3, 4$), the condensate density exhibits an exponential tail. For $g \geq 5$, the condensate spans the entire domain, indicating a delocalized state. In panel (b), the red dashed line shows a double-exponential fit to the ground-state density for $g = 0$.

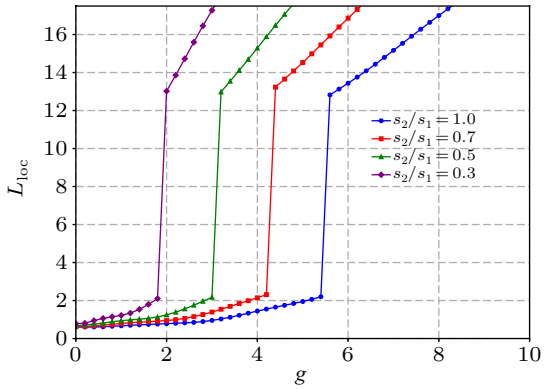


Fig. 2. Variation of the localization length $L_{\rm loc}$ with the nonlinearity for different s_2/s_1 ratios. The localization length $L_{\rm loc}$ is calculated from the $1/\mathrm{e}$ decay of the fitted curve $ae^{-|x-x_0|/L_{\rm loc}} + ae^{-|x+x_0|/L_{\rm loc}}$, where x_0 denotes the position of maximum density in space. Here $x_0 = \pm 2.275$. The localization length $L_{\rm loc}$ starts to increase beyond the critical nonlinearity $g_{\rm c}$, and $g_{\rm c}$ increases with increasing s_2/s_1. The other parameters are the same as those in Fig. 1.

To quantify this localization–delocalization transition, the localization length $L_{\rm loc}$ is computed by fitting the localized states with the function $y = a\exp(-|x-x_0|/L_{\rm loc}) + a\exp(-|x+x_0|/L_{\rm loc})$, where a is a fitting parameter, x_0 denotes the localization center, and $L_{\rm loc}$ is the localization length. The variation of $L_{\rm loc}$ with respect to g is plotted in Fig. 2 for different values of s_2/s_1. We find that when the condensate is in the localized state, $L_{\rm loc}$ varies linearly with g. However, a discontinuous jump occurs in $L_{\rm loc}$ at a critical value of g, beyond which delocalization appears in the density profile. The threshold value of the nonlinearity at which delocalization occurs decreases as the disorder strength s_2/s_1 decreases.

These ground states correspond to a conservative, closed-system setting, explicitly ignoring the reservoir. This approach provides initial conditions for the open-system quench dynamics discussed in subsequent sections. The key carry-over aspect is the localized-to-delocalized crossover phenomenology: exponential tails at small g persist as stable propagation in open dynamics, whereas extended profiles at large g seed breathing or chaotic instabilities modulated by dissipation.

The physical mechanism driving delocalization as g increases involves competition between quasiperiodic interference-induced localization (Anderson-like, where destructive interference traps the wavefunction in potential minima) and interaction-induced density redistribution. In the non-interacting limit, the quasiperiodic potential induces localization via wave interference. As g increases, the term $g|\psi|^2$ acts as an effective potential that redistributes the condensate density, thereby partially screening the underlying disorder and weakening its localizing effect. This is akin to interaction-driven delocalization in quasiperiodic Bose–Hubbard models.[52] In our finite system with hard-wall boundaries, "delocalized" means that the density profile spans the entire computational domain without exponential tails (i.e., the localization length $L_{\rm loc}$ is comparable to the system size L), although boundaries prevent true infinite delocalization.

3.2. Quench dynamics

Following the characterization of the ground-state transition in Subsection 3.1, we conduct dynamical simulations of an interacting exciton–polariton condensate in a one-dimensional quasi-periodic optical lattice to investigate the detailed dynamics of localized and delocalized condensates. We systematically explore the emergence of chaos triggered by quenching the interaction strength. By numerically solving the reservoir-coupled GP Eqs. (4) and (5), we map the spatiotemporal evolution of the condensate for various interaction strengths g and reservoir decay rates $\bar{\gamma}_{\rm R}$.

Under the condition of a fixed reservoir decay rate $\bar{\gamma}_{\rm R} = 14$, we analyze the density evolution of the system for various initial interaction strengths that are subsequently quenched to zero. The results are depicted in Figs. 3(a) and 3(b). It is observed that when the initial interaction strength is relatively weak, the system remains in a localized state even after quenching the interaction parameter g to zero. Conversely, when the initial interaction strength is stronger, the system

transitions to an extended state following the quench. In contrast, pronounced breathing-like oscillations are observed when the condensate is initially prepared at $g = 6$, as shown in Fig. 3(b).

The effect of varying $\bar{\gamma}_R$ is further examined, with the interaction strength fixed at $g = 2$. For $\bar{\gamma}_R = 14$, the localized condensate again propagates without distortion, as illustrated in Fig. 3(a). However, for a lower decay rate of $\bar{\gamma}_R = 3$, the condensate exhibits pronounced breathing oscillations, as seen in Fig. 3(c). The same behavior is observed when comparing Fig. 3(b) with Fig. 3(d).

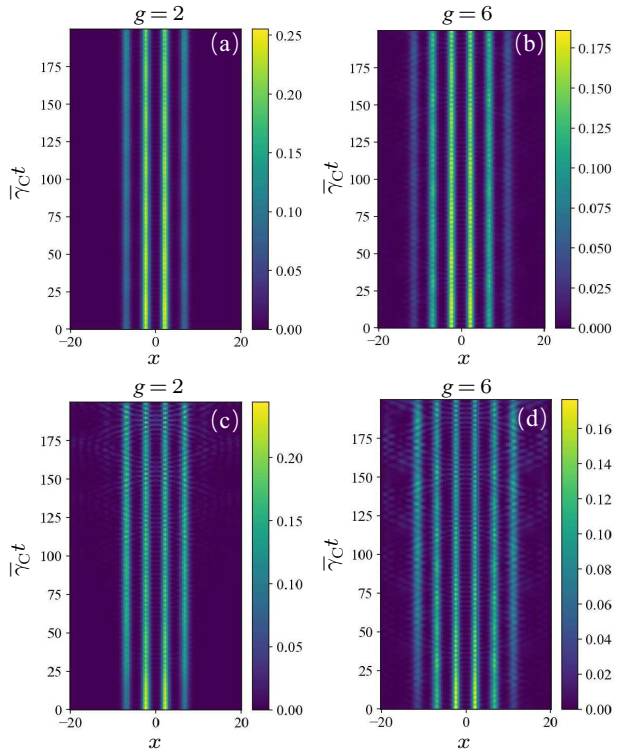


Fig. 3. Time evolution of the condensate density $|\psi(x,t)|^2$, calculated using Eqs. (4) and (5) after quenching the nonlinearity to zero, for different values of g and $\bar{\gamma}_R$: (a) $g = 2$, $\bar{\gamma}_R = 14$; (b) $g = 6$, $\bar{\gamma}_R = 14$; (c) $g = 2$, $\bar{\gamma}_R = 3$; and (d) $g = 6$, $\bar{\gamma}_R = 3$. The other parameters are $\bar{\gamma}_C = 1$ and $\bar{R} = 0.5$.

The transition between dynamical regimes exhibits a systematic dependence on system parameters. To quantify the role of dissipation, localization properties are compared for two reservoir decay rates: $\bar{\gamma}_R = 14$ and $\bar{\gamma}_R = 3$. A higher value of $\bar{\gamma}_R$ consistently suppresses breathing oscillations and promotes dynamical localization, as stronger dissipation damps nonlinear excitations and stabilizes the condensate against chaotic spreading. The stimulated scattering rate is set to $\bar{R} = 0.5$, placing the system in a moderate-coupling regime where both localized and delocalized phases are accessible by tuning g. This parameter choice allows the full phase diagram to be explored without being restricted to either the strongly dissipative or the weakly nonlinear limit.

The incorporation of a reservoir n_R significantly impacts the steady-state properties of the exciton–polariton condensate. In the absence of the reservoir, when interactions are relatively weak, the ground state of the system is typically localized. However, upon incorporating the reservoir and allowing the system to evolve dynamically, the ground state may transition from a localized to a delocalized state. Conversely, if the initial ground state is delocalized, the introduction of the reservoir and subsequent dynamical evolution can lead to localization. This behavior underscores the crucial role of the interaction between the reservoir and polaritons in modulating the spatial coherence and overall state of the exciton–polariton condensate.

To further elucidate the oscillatory (breathing) features observed in the density evolution in Fig. 3, and to establish a direct connection to the subsequent analyses based on $c(t)$, PSD, and λ_{max}, we quantify the breathing dynamics by tracking the time-dependent amplitude of a representative mode. Specifically, we integrate the intensity $|\psi(x,t)|^2$ over a narrow spatial window centered on the dominant density peak to the left of $x = 0$ (typically located at $x \approx -2.4$), which corresponds to the most prominent bright stripe visible in the spatiotemporal plots. This amplitude serves as a direct proxy for the breathing motion of the localized condensate and captures its instability without interference from global effects.

Figure 4 shows the temporal evolution of this amplitude for four representative cases covering weak and strong nonlinearity (g) as well as high and low reservoir dissipation ($\bar{\gamma}_R$). For weak nonlinearity and high dissipation, as illustrated in Fig. 4(a), the amplitude displays nearly periodic oscillations with a stable envelope, consistent with the undistorted propagation of localized condensates seen in Fig. 3.

With increasing nonlinearity, as illustrated in Fig. 4(b), the breathing amplitude develops modulated oscillations with noticeable irregular variations, reflecting the onset of frequency mixing. The PSD shows broader peaks together with elevated background noise, mirroring the spectral broadening observed in $c(t)$ and correlating with faster and more irregular decay of $c(t)$. Lowering the dissipation rate further enhances this trend: at low $\bar{\gamma}_R$ and weak g, as illustrated in Fig. 4(c), the appearance of minor amplitude modulations suggests a transition toward quasi-periodic regimes. Finally, under combined strong nonlinearity and low dissipation, as illustrated in Fig. 4(d), the amplitude becomes highly erratic. This regime corresponds to positive $\lambda_{max} > 0.12$, marking the onset of chaos, where nonlinearity drives mode instability.

This quantitative analysis directly bridges the real-space breathing features observed in Fig. 3 to the chaos diagnostics employed later in the manuscript: the progressive destabilization of the breathing mode, manifested in amplitude irregularities and PSD evolution, underlies the decay of $c(t)$, the broadening of its spectrum, and the emergence of positive λ_{max}. These results highlight the cooperative interplay between nonlinearity and dissipation in determining the system's dynamical transition.

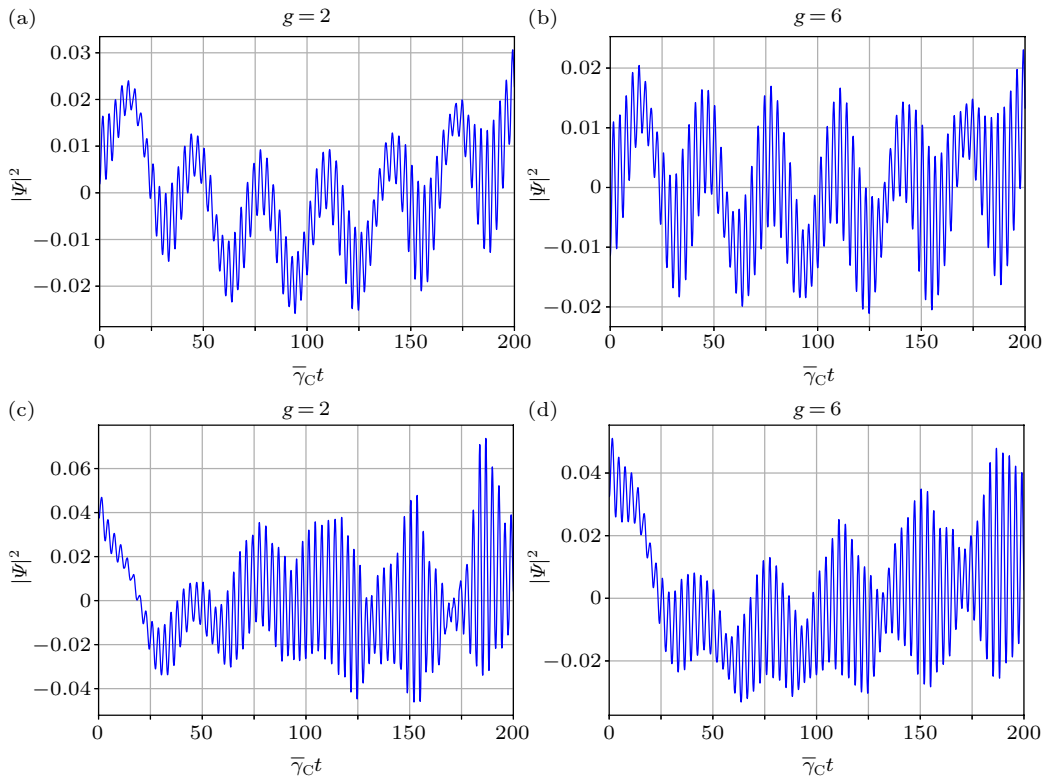


Fig. 4. Temporal evolution of the breathing amplitude (obtained by integrating $|\psi(x,t)|^2$ over the dominant density peak to the left of $x = 0$) for different values of the nonlinearity g and reservoir dissipation $\bar{\gamma}_R$. (a) $g = 2$, $\bar{\gamma}_R = 14$: Nearly periodic oscillations indicative of regular dynamics. (b) $g = 6$, $\bar{\gamma}_R = 14$: Modulated breathing with irregular amplitude variations, signaling the onset of instability. (c) $g = 2$, $\bar{\gamma}_R = 3$: Slight modulations emerge under reduced dissipation, indicating a transition toward quasi-periodicity. (d) $g = 6$, $\bar{\gamma}_R = 3$: Highly erratic fluctuations, corresponding to chaotic behavior with broadband spectral content.

3.3. Correlation and dynamical behaviors

In this subsection, we introduce the time-correlator function $c(t)$[53,54] to investigate the impact of nonlinear interactions and dissipative effects on the system's transition to chaotic dynamics. The function is defined as

$$c(t) = |\langle \psi(x,0) | \tilde{\psi}(x,t) \rangle| \tag{6}$$

where $\psi(x,0)$ denotes the ground state obtained through imaginary-time propagation under repulsive interactions, and $\tilde{\psi}(x,t) = \psi(x,t)/\sqrt{N(t)}$, with $N(t)$ being the normalized particle number derived from the time evolution of $\psi(x,0)$.

Owing to the reservoir equation $n_R(x,t)$, which induces variations in the particle number, the initial stability of $c(t)$ is compromised. Consequently, we allow the system to evolve according to Eqs. (4) and (5) for a sufficiently long time and then use the resulting steady state for quantitative analysis. In the localized regime ($g \leq 4$), $c(t)$ exhibits periodic or quasi-periodic oscillations, indicating coherent dynamics, as shown in Figs. 5(a)–5(d). The regularity of these oscillations reflects the stability of the localized ground state, while the systematic variation of their period with g suggests a tunable coherent response. As the system transitions into the delocalized regime ($g \geq 5$), $c(t)$ loses periodicity and displays irregular fluctuations, a hallmark of chaotic dynamics, as shown in Figs. 5(e) and 5(f). This behavior directly reflects the complex interplay between nonlinear interactions and dissipative processes in the extended state.

These results demonstrate that quenching the nonlinearity can induce periodic, quasi-periodic, or chaotic temporal evolution, depending on whether the underlying ground state is localized or delocalized.

To further investigate the frequency content of the dynamics and the route to chaotic behavior in the delocalized regime, we compute the PSD of the time correlator, which is given by[55]

$$\mathrm{PSD}(\omega) = \frac{|\hat{c}(\omega)|^2}{2\pi N}, \tag{7}$$

where $\hat{c}(\omega)$ is the discrete Fourier transform of the time correlator $c(t)$.

The PSD for different values of g is shown in Fig. 6, providing clear evidence of the localization–delocalization transition. In the localized regime ($g = 1, 2, 3$), the spectra exhibit discrete peaks at a fundamental frequency and its harmonics, confirming periodic dynamics, as shown in Figs. 6(a)–6(c). The systematic shift of the dominant peak with increasing g reflects the tunability of the coherent oscillatory response. At $g = 4$, additional frequency components emerge, indicating the onset of quasi-periodic dynamics and foreshadowing the transition toward chaos, as shown in Fig. 6(d). In the delocalized

regime ($g = 5, 6$), the spectra become continuous and broadband, featuring numerous intertwined peaks — a hallmark of chaotic evolution — as shown in Figs. 6(e) and 6(f). This transformation demonstrates that the system enters a complex, aperiodic temporal state driven by the interplay of interactions and the underlying quasi-periodic potential.

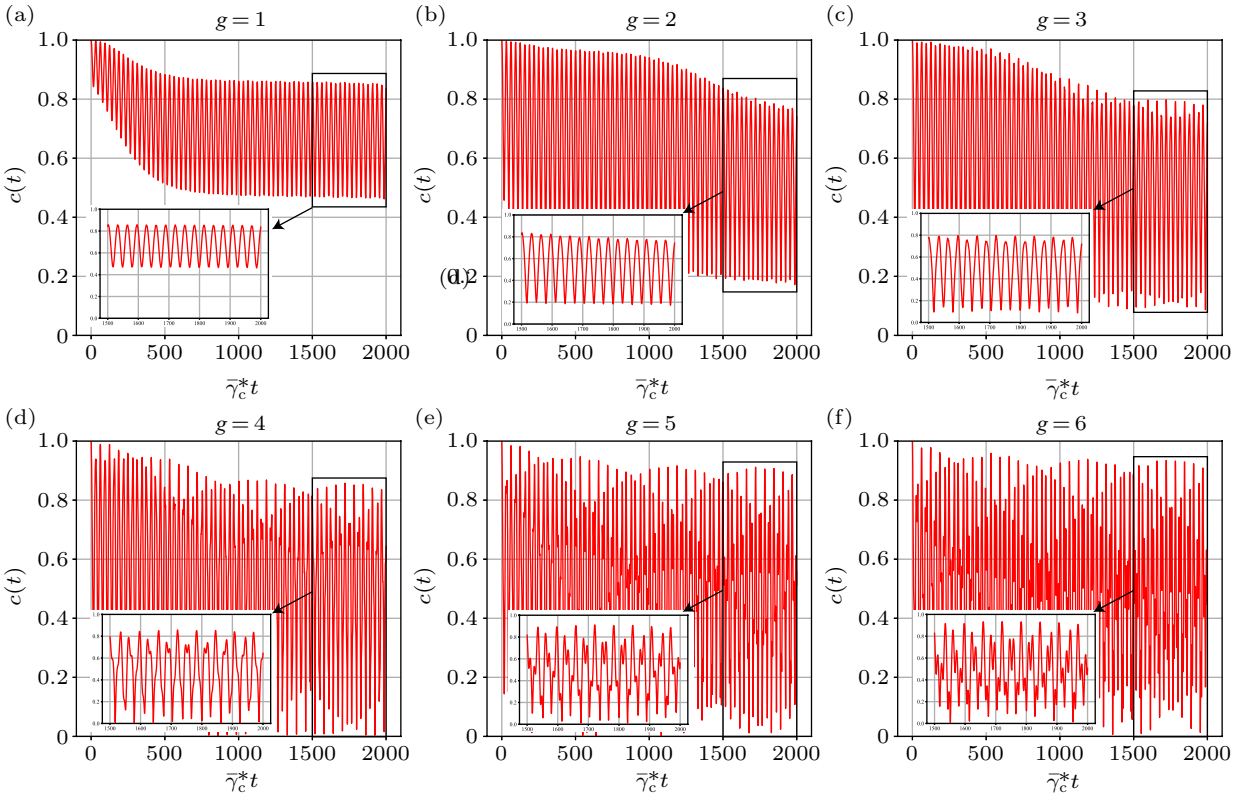


Fig. 5. Temporal variation of the time-correlation function $c(t)$ calculated using Eq. (6) at $s_2/s_1 = 1.0$, $s_1 = 3$, $\lambda_1 = 10.0$, and $\bar{\gamma}_R = 14$ for different nonlinearities: (a) $g = 1$, (b) $g = 2$, (c) $g = 3$, (d) $g = 4$, (e) $g = 5$, and (f) $g = 6$. The horizontal axis represents time t, with data shown up to $t = 2000$, while the vertical axis shows the amplitude of the time-dependent ground-state autocorrelation function $c(t)$. The six panels, ordered from top to bottom and left to right, correspond to $g = 1, 2, 3, 4, 5, 6$. The insets (blue framed regions) show the evolution of $c(t)$ in the time window $t \in [1500, 2000]$, highlighting the late-time decay behavior. These results illustrate the transition from localized ($g \leq 4$) to delocalized ($g \geq 5$) regimes.

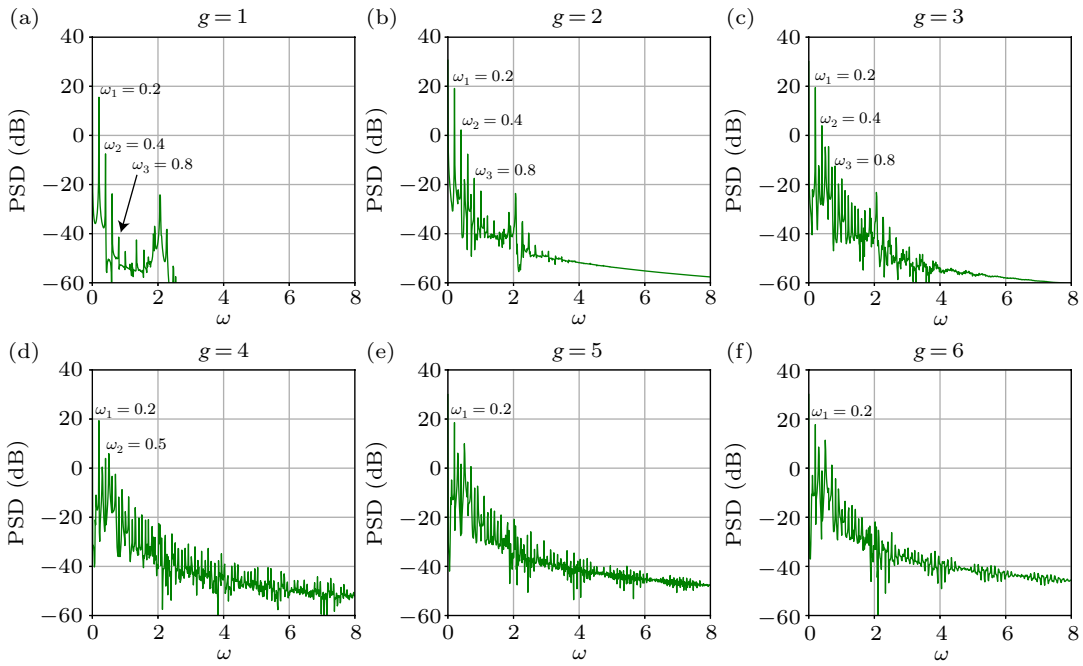


Fig. 6. PSD calculated using Eq. (7) of the time-correlation function (Fig. 3) for different nonlinearities: (a) $g = 1$ (periodic), (b) $g = 2$ (periodic), (c) $g = 3$ (periodic), (d) $g = 4$ (quasi-periodic), (e) $g = 5$ (chaotic), and (f) $g = 6$ (chaotic). The remaining parameters are identical to those in Fig. 3. As the nonlinearity increases, two incommensurate frequencies $\omega_1 = 0.20$ and $\omega_2 = 0.5$ emerge at $g = 4$. At higher nonlinearity ($g \geq 5$), a large number of frequencies are generated, indicating broadband spectra and a signature of chaotic dynamics.

3.4. Lyapunov exponent

In this subsection, we establish a connection between delocalization and chaos by computing the maximal Lyapunov exponent. In dynamical systems, Lyapunov exponents characterize the mean exponential rate of divergence between two nearby trajectories. In phase space, the evolution of an infinitesimal initial separation δX_0 can be expressed as[56]

$$|\delta X(t)| \approx \mathrm{e}^{\lambda t}\,|\delta X_0|, \tag{8}$$

$$\lambda_{\max} = \lim_{t\to\infty} \frac{1}{t} \ln \frac{|\delta X(t)|}{|\delta X_0|}, \tag{9}$$

where $|\delta X(t)|$ denotes the Euclidean (or chosen) norm of the perturbation at time t, δX_0 is the initial perturbation vector, and λ is the instantaneous exponential growth rate.

Dynamical simulations of an interacting exciton–polariton condensate in a one-dimensional quasiperiodic optical lattice are performed to systematically investigate chaos induced by quenching the interaction strength and varying the reservoir decay rate. The stable time window of $c(t)$ (as shown in the inset of Fig. 5) is selected to compute the maximal Lyapunov exponent $\lambda_{\max}$ for different values of g and $\bar{\gamma}_{\mathrm{R}}$. A chaos phase diagram is constructed, revealing a clear connection between localization and chaotic dynamics. The phase diagram (Fig. 7(a)) illustrates the competition between interactions and dissipation. In the weak-interaction regime ($g \leq 2.0$), Anderson localization dominates: the wave function remains exponentially localized, the dynamics is regular, and the maximal Lyapunov exponent satisfies $\lambda_{\max} \approx 0$. As the interaction strength increases, nonlinear effects progressively disrupt localization, driving the system into a transitional regime. In the strong-interaction regime ($g \geq 4.0$), the system becomes fully delocalized and exhibits pronounced chaotic dynamics, characterized by large positive values of $\lambda_{\max}$.

In Fig. 7(b), with g fixed at 2.8, we observe that $\bar{\gamma}_{\mathrm{R}}$ plays a crucial role in determining the system's state. For small $\bar{\gamma}_{\mathrm{R}}$, the reservoir enhances instability and drives the system into chaos. Conversely, for large $\bar{\gamma}_{\mathrm{R}}$, dissipation suppresses fluctuations and stabilizes the dynamics. In Fig. 7(c), with $\bar{\gamma}_{\mathrm{R}}$ fixed at 5, the interaction strength g remains the dominant control parameter: increasing g enhances instability and promotes chaotic behavior, consistent with typical exciton–polariton condensate dynamics.

To summarize, the system is stable when the interaction strength g is small or when the reservoir-induced damping $\bar{\gamma}_{\mathrm{R}}$ is sufficiently large. Conversely, chaotic behavior emerges when g exceeds a critical threshold or when $\bar{\gamma}_{\mathrm{R}}$ becomes too weak. The introduction of a reservoir in exciton–polariton systems therefore provides a tunable pathway for controlling quantum state dynamics.

For small nonlinearity ($g \leq 2$), the ground-state stability is not yet broken, so $\lambda_{\max}$ remains close to zero and the correlation function decays regularly. As g increases, phase-space stretching induced by nonlinearity becomes significant: the correlation function develops irregular oscillations and $\lambda_{\max}$ increases. The onset of chaotic behavior at $g \approx 4$ indicates a critical point separating distinct dynamical regimes. Near this point, the system exhibits enhanced sensitivity to parameter variations and the emergence of complex dynamics.

It is noteworthy that the reservoir decay rate $\bar{\gamma}_{\mathrm{R}}$ plays a dual role in controlling chaos. Both too weak and too strong dissipation suppress chaotic dynamics, whereas an intermediate regime $5 \leq \bar{\gamma}_{\mathrm{R}} \leq 14$ allows dissipation and nonlinearity to balance dynamically, sustaining a pronounced positive Lyapunov exponent region. Within the framework of open quantum systems, environmental coupling introduces additional dissipation channels that damp coherent evolution and thereby reduce the degree of chaos.

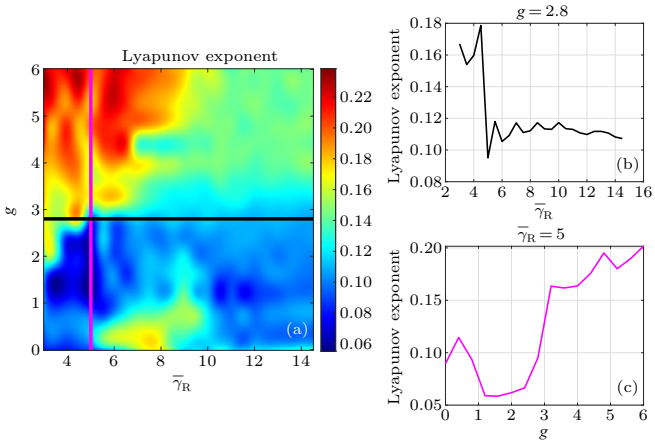


Fig. 7. The color map in (a) displays $\lambda_{\max}$ calculated using Eqs. (8) and (9) as a function of the two dimensionless control parameters: g (vertical axis) and $\bar{\gamma}_{\mathrm{R}}$ (horizontal axis). The color bar encodes the magnitude of $\lambda_{\max}$ — red/orange regions indicate large positive values (chaotic dynamics), while blue regions correspond to small values of $\lambda_{\max}$ (nearly regular, non-chaotic behavior). In panel (b), keeping $g = 2.8$, we show the dependence of the Lyapunov exponent on $\bar{\gamma}_{\mathrm{R}}$. In panel (c), keeping $\bar{\gamma}_{\mathrm{R}} = 5$, we plot the nonlinear dependence of $\lambda_{\max}$ on g. A sharp transition occurs near $g_{\mathrm{c}} = 2.5$. The reservoir decay rate acts as a damping control: below a critical threshold $\bar{\gamma}_{\mathrm{R}}^{\mathrm{c}}$ (5–10), moderate $\bar{\gamma}_{\mathrm{R}}$ cooperates with g to open a wide tunable chaotic window; above $\bar{\gamma}_{\mathrm{R}}^{\mathrm{c}}$, strong damping universally suppresses chaos, independent of g, by quenching nonlinear growth.

4. Discussion

In summary, we establish that chaos in open polariton–nonlinear systems is governed by a cooperative control provided by g and $\bar{\gamma}_{\mathrm{R}}$. A two-dimensional parameter scan quantitatively maps the chaotic boundary, revealing that moderate dissipation lowers the onset threshold by an order of magnitude and significantly widens the experimentally accessible chaotic window. Conversely, strong dissipation rapidly suppresses fluctuations and restores regular dynamics.

This cooperative interplay highlights a key difference from closed nonlinear systems — such as pure Bose–Einstein condensates without a reservoir — where chaos typically requires very strong nonlinearities and is highly sensitive to pa-

rameter variations. In our open system, the introduction of $\bar{\gamma}_R$ not only shifts the onset of chaos toward moderate nonlinearities but also substantially enlarges the chaotic domain, making it more robust and experimentally accessible.

Our work identifies and quantifies this cooperative mechanism: chaos is not determined by a single parameter but emerges from the joint action of nonlinearity and dissipation. This contrasts with earlier studies of open systems (e.g., optical-lattice models coupled to baths), which often focused on single-parameter variations and sometimes reported that extreme dissipation ($\bar{\gamma}_R \to \infty$) completely suppresses chaos. In our setup, however, total density conservation prevents complete system depletion, enabling a continuous and reversible transition between chaotic and regular regimes as g and $\bar{\gamma}_R$ are varied. Such deterministic control offers a practical experimental tool, particularly in cold-atom and polariton-circuit platforms, where both interaction strength and reservoir coupling can be independently tuned.

From a theoretical perspective, our findings illuminate the dual role of dissipation: while strong damping stabilizes the system, moderate damping can actively assist the emergence of chaos under nonlinear interactions. This cooperative mechanism reshapes the understanding of open-system dynamics, demonstrating that dissipation can act as a chaos generator rather than merely a suppressor. The resulting wide and tunable chaotic window opens pathways for applications in quantum-information protocols, such as chaotic encryption, where deterministic switching between chaotic and regular regimes is essential. Ultimately, this study underscores the importance of parameter cooperation in open quantum and optical systems, providing a unified framework to explore chaos and stability across diverse experimental platforms. The demonstrated cooperative control may also inform the exploration of other non-equilibrium quantum phases, such as the room-temperature polariton supersolidity recently proposed in guided parametric systems.[57]

Regarding experimental feasibility, the predicted wide and tunable chaotic window is readily accessible with current exciton–polariton platforms. The nonlinearity g can be tuned over more than an order of magnitude by varying the non-resonant pump intensity or the cavity–exciton detuning, both standard techniques in GaAs- and TMD-based microcavities. The effective reservoir decay rate $\bar{\gamma}_R$ can be controlled via material choice (inorganic vs. organic semiconductors with different exciton lifetimes), operating temperature, or cavity quality factor. Recent experiments have already demonstrated tunable chaotic and turbulent dynamics as well as quench protocols in polariton condensates within comparable parameter regimes.[53,58,59] Our cooperative g–$\bar{\gamma}_R$ mechanism can therefore be directly probed using existing all-optical lattice setups and time-resolved photoluminescence techniques, opening concrete pathways toward chaotic encryption and ultrafast signal processing in polaritonic devices.

Acknowledgments

Project supported by the National Natural Science Foundation of China (Grant No. 12404362), the Fundamental Research Funds for the Central Universities (Grant No. JUSRP123027), the National Natural Science Foundation of China (Grant No. 12264061), Excellent Youth Funding of Hunan Provincial Education Department (Grant No. 24B0807), and Hunan Provincial Natural Science Foundation of China (Grant No. 2025JJ70330).

References

[1] Deng H, Haug H and Yamamoto Y 2010 *Rev. Mod. Phys.* **82** 1489
[2] Keeling J and Berloff N G 2011 *Contemp. Phys.* **52** 131
[3] Shelykh I A, Kavokin A V, Rubo Y G, Liew T C H and Malpuech G 2010 *Semicond. Sci. Technol.* **25** 013001
[4] Gao W, Li X, Bamba M and Kono J 2018 *Nat. Photonics* **12** 362
[5] Nada M Y, Othman M A K and Capolino F 2017 *Phys. Rev. B* **96** 184304
[6] Khurgin J B 2020 *Optica* **7** 1015
[7] Wingenbach J, Schumacher S and Ma X 2024 *Phys. Rev. Res.* **6** 013148
[8] Su R, Ghosh S, Wang J, Liu S, Diederichs C, Liew T C H and Xiong Q 2020 *Nat. Phys.* **16** 301
[9] Lerario G, Fieramosca A, Barachati F, Ballarini D, Daskalakis K S, Dominici L, Giorgi M D, Maier S A, Gigli G, Kéna-Cohen S and Sanvitto D 2017 *Nat. Phys.* **13** 837
[10] Song H G, Choi S, Park C H, Gong S H, Lee C, Kwon M S, Choi D G, Woo K Y and Cho Y H 2019 *Optica* **6** 1313
[11] Song J, Ghosh S, Deng X, Li C, Shang Q, Liu X, Wang Y, Gao X, Yang W, Wang X, Zhao Q, Shi K, Gao P, Xing G, Xiong Q and Zhang Q 2025 *Sci. Adv.* **11** eadr1652
[12] Lackner L, Dusel M, Egorov O A, Han B, Knopf H, Eilenberger F, Schröder S, Watanabe K, Taniguchi T, Tongay S, Anton-Solanas C, Höfling S and Schneider C 2021 *Nat. Commun.* **12** 4933
[13] Zhu T, Chen Z, Wang X, Huang Z, Zhao H and Wang J 2025 *Chin. Phys. B* **34** 094202
[14] Zhang X, Zhang T, Lu M H and Chen Y F 2022 *Adv. Phys. X* **7** 2109431
[15] Pinsker F and Flayac H 2014 *Phys. Rev. Lett.* **112** 140405
[16] Winkler K, Fischer J, Schade A, Amthor M, Dall R, Geßler J, Emmerling M, Ostrovskaya E A, Kamp M, Schneider C and Höfling S 2015 *New J. Phys.* **17** 023001
[17] Schneider C, Winkler K, Fraser M D, Kamp M, Yamamoto Y, Ostrovskaya E A and Höfling S 2016 *Rep. Prog. Phys.* **80** 016503
[18] Lai C W, Kim N Y, Utsunomiya S, Roumpos G, Deng H, Fraser M D, Byrnes T, Recher P, Kumada N, Fujisawa T and Yamamoto Y 2007 *Nature* **450** 529
[19] Krizhanovskii D N, Cerda-Méndez E A, Gavrilov S, Sarkar D, Guda K, Bradley R, Santos P V, Hey R, Biermann K, Sich M, Fras F and Skolnick M S 2013 *Phys. Rev. B* **87** 155423
[20] Chestnov I Y, Yulin A V, Alodjants A P and Egorov O A 2016 *Phys. Rev. B* **94** 094306
[21] del Valle-Inclan Redondo Y, Schneider C, Klembt S, Höfling S, Tarucha S and Fraser M D 2023 *Nano Lett.* **23** 4564
[22] del Valle-Inclan Redondo Y, Xu X, Liew T C H, Ostrovskaya E A, Stegmaier A, Thomale R, Schneider C, Dam S, Klembt S, Höfling S, Tarucha S and Fraser M D 2024 *Nat. Photonics* **18** 548
[23] Dai Z B, Fan H, Semenenko V, Lv X, Wen L, Zhang Z, Fang S, Perebeinos V, Zhao Y and Li Z 2024 *Sci. Adv.* **10** eadq7445
[24] Xie S, Tu L, Han Y, Huang L, Kang K, Lao K U, Poddar P, Park C, Muller D A, DiStasio R A and Park J 2018 *Science* **359** 1131
[25] Cerda-Méndez E A, Krizhanovskii D N, Biermann K, Hey R, Skolnick M S and Santos P V 2012 *New J. Phys.* **14** 075011
[26] Ai Q, Wingenbach J, Yang X, Wei J, Hatzopoulos Z, Savvidis P G, Schumacher S, Ma X and Gao T 2025 *Phys. Rev. Appl.* **23** 024029

[27] Wang D, Xiong A Y, Zhang J Q, She Z, Kang X, Zhu Y, Ghosh S and Xiong Q 2024 *Chin. Phys. B* **33** 128103
[28] Bao R, Xu H, Verstraelen W and Liew T C H 2023 *Phys. Rev. B* **108** 235305
[29] Zhang Y, Jia C and Liang Z 2022 *Chin. Phys. Lett.* **39** 020501
[30] Xu X, Tian L, An Z, Xiong Q and Ghosh S 2025 *Phys. Rev. B* **111** L121301
[31] Xu X, Liu H, Zhang Z and Liang Z 2020 *J. Phys. Condens. Matter* **32** 425402
[32] Chen L, Niu Z X and Xu X 2024 *Sci. Rep.* **14** 21745
[33] Estrecho E, Gao T, Bobrovska N, Comber-Todd D, Fraser M D, Steger M, West K, Pfeiffer L N, Levinsen J, Parish M M, Liew T C H, Matuszewski M, Snoke D W, Truscott A G and Ostrovskaya E A 2019 *Phys. Rev. B* **100** 035306
[34] Chen W, Kaya Ozdemir S, Zhao G, Wiersig J and Yang L 2017 *Nature* **548** 192
[35] Koniakhin S, Bleu O, Malpuech G and Solnyshkov D 2020 *Chaos Solitons Fractals* **132** 109574
[36] Jia C, Wu R, Hu Y, Liu W M and Liang Z 2021 *Front. Phys.* **9** 805841
[37] Takemura N, Trebaol S, Wouters M, Portella-Oberli M T and Deveaud B 2014 *Nat. Phys.* **10** 500
[38] Navadeh-Toupchi M, Takemura N, Anderson M D, Oberli D Y and Portella-Oberli M T 2019 *Phys. Rev. Lett.* **122** 047402
[39] Xu X, Chen L, Zhang Z and Liang Z 2018 *J. Phys. B: At. Mol. Opt. Phys.* **52** 025303
[40] Helluin F, Pinto-Dias D, Fontaine Q, Ravets S, Bloch J, Minguzzi A and Canet L 2025 *Phys. Rev. Res.* **7** 033103
[41] Miri M A and Alu A 2019 *Science* **363** eaar7709
[42] Gao T, Estrecho E, Bliokh K Y, Liew T C H, Fraser M D, Brodbeck S, Kamp M, Schneider C, Höfling S, Yamamoto Y, Nori F, Kivshar Y S, Truscott A G, Dall R G and Ostrovskaya E A 2015 *Nature* **526** 554
[43] Sturges T J, Anderson M D, Buraczewski A, Navadeh-Toupchi M, Adiyatullin A F, Jabeen F, Oberli D Y, Portella-Oberli M T and Stobinska M 2019 *Sci. Rep.* **9** 19396
[44] Nikitin A V and Zezyulin D A 2024 *Phys. Rev. B* **109** 085304
[45] Carusotto I and Ciuti C 2013 *Rev. Mod. Phys.* **85** 299
[46] Wouters M and Carusotto I 2007 *Phys. Rev. Lett.* **99** 140402
[47] Roati G, D'Errico C, Fallani L, Fattori M, Fort C, Zaccanti M, Modugno G, Modugno M and Inguscio M 2008 *Nature* **453** 895
[48] Smirnov L A, Smirnova D A, Ostrovskaya E A and Kivshar Y S 2014 *Phys. Rev. B* **89** 235310
[49] Jouzdani P, Johnson C W, Mucciolo E R and Stetcu I 2022 *Phys. Rev. A* **106** 062435
[50] Symons B C B, Manawadu D, Galvin D and Mensa S 2024 *Phys. Rev. B* **110** 174302
[51] Bauer N M, Alam R, Siopsis G and Ostrowski J 2024 *Phys. Rev. A* **109** 052430
[52] Znidaric M and Ljubotina M 2018 *Proc. Natl. Acad. Sci. USA* **115** 4595
[53] Ruiz-Sánchez R, Rechtman R and Rubo Y G 2020 *Phys. Rev. B* **101** 155305
[54] Song Y, Zou D, Gat O, Hu M and Grelu P 2023 *Laser Photonics Rev.* **17** 2300066
[55] Dalui S, Majhi B R and Mishra P 2020 *Int. J. Mod. Phys. A* **35** 2050081
[56] Brezinova I, Collins L A, Ludwig K, Schneider B I and Burgdörfer J 2011 *Phys. Rev. A* **83** 043611
[57] Tian L, Gan Y, Shi Y, Xu L, Xu H and Xiong Q 2025 *Chin. Phys. Lett.* **42** 090405
[58] Ferrini R and Koniakhin S V 2025 *Phys. Rev. B* 112
[59] Baboux F, De Bernardis D, Goblot V, Gladilin V N, Gomez C, Galopin E, Le Gratiet L, Lemaitre A, Sagnes I, Carusotto I, Wouters M, Amo A and Bloch J 2018 *Optica* **5** 1163